Development of a Practical Secondary Control for Hardware Microgrids

Preprint

Soham Chakraborty, Jing Wang, Subhankar Ganguly, and Benjamin Kroposki

National Renewable Energy Laboratory

Presented at the 2024 IEEE Energy Conversion Congress & Expo (ECCE)
Phoenix, Arizona
October 20–24, 2024

NREL is a national laboratory of the U.S. Department of Energy
Office of Energy Efficiency & Renewable Energy
Operated by the Alliance for Sustainable Energy, LLC

This report is available at no cost from the National Renewable Energy Laboratory (NREL) at www.nrel.gov/publications.

Contract No. DE-AC36-08GO28308

Conference Paper
NREL/CP-5D00-89097
December 2024

Development of a Practical Secondary Control for Hardware Microgrids

Preprint

Soham Chakraborty, Jing Wang, Subhankar Ganguly, and Benjamin Kroposki

National Renewable Energy Laboratory

Suggested Citation
Chakraborty, Soham, Jing Wang, Subhankar Ganguly, and Benjamin Kroposki. 2024. *Development of a Practical Secondary Control for Hardware Microgrids: Preprint*. Golden, CO: National Renewable Energy Laboratory. NREL/CP-5D00-89097. https://www.nrel.gov/docs/fy25osti/89097.pdf.

NREL is a national laboratory of the U.S. Department of Energy
Office of Energy Efficiency & Renewable Energy
Operated by the Alliance for Sustainable Energy, LLC

This report is available at no cost from the National Renewable Energy Laboratory (NREL) at www.nrel.gov/publications.

Contract No. DE-AC36-08GO28308

Conference Paper
NREL/CP-5D00-89097
December 2024

National Renewable Energy Laboratory
15013 Denver West Parkway
Golden, CO 80401
303-275-3000 • www.nrel.gov

NOTICE

This work was authored by the National Renewable Energy Laboratory, operated by Alliance for Sustainable Energy, LLC, for the U.S. Department of Energy (DOE) under Contract No. DE-AC36-08GO28308. Funding provided by the U.S Department of Energy Office of Energy Efficiency and Renewable Energy Solar Energy Technologies Office Agreement Number 38637. The views expressed herein do not necessarily represent the views of the DOE or the U.S. Government.

Development of a Practical Secondary Control for Hardware Microgrids

Soham Chakraborty, Jing Wang, Subhankar Ganguly, Benjamin Kroposki
Power Systems Engineering Center, National Renewable Energy Laboratory, Golden, Colorado 80401, USA.
{soham.chakraborty, jing.wang, subhankar.ganguly, benjamin.kroposki}@nrel.gov

***Abstract*—Practical, vendor-agnostic interoperability guidelines for the *secondary control* architecture of microgrids (MGs) with multiple grid-forming (GFM) inverter-based resources (IBRs) have not yet been developed. Therefore, this paper proposes a generic and vendor-agnostic secondary control architecture that operates with all GFM IBRs and synchronous generators. This secondary control does not require the use of additional measurement devices in the MG and utilizes the inherent communication systems of the GFM units, such as Modbus TCP/IP. The practical challenges of Modbus registers, such as packet loss and quantization error, and their detrimental impacts on *secondary control* actions are investigated. The proposed three-stage modification for any *secondary control* architecture to mitigate these impacts includes: 1) averaging the data read, 2) situational event-triggering of the controller, and 3) finite iteration of the controlling action. The proposed method is validated using a 3-ϕ, 480 V, 60 Hz, 500 kVA laboratory hardware microgrid with commercial two GFM IBRs and one diesel generator. The experimental results corroborates the fact the proposed modification in the *secondary control* architecture is advantageous for practical usage under erroneous measurements.**

I. Introduction

A microgrid (MG) is defined as "a group of interconnected loads and distributed energy resources (DERs) with clearly defined electrical boundaries that acts as a single controllable entity with respect to the grid and can connect and disconnect from the grid to enable it to operate in both grid-connected or island modes" [1]. Various renewable-based (PV panels, wind farms, etc.) and storage-based (battery energy, fuel-cell, etc.) energy resources are interfaced to MGs usually via voltage-source inverters and those DERs are called as inverter-based resources (IBRs). MGs are able to operate both in grid-connected and islanded modes, leveraged by a hierarchical control architecture. To adapt ANSI/ISA-95, or ISA-95, a four layer MG control architecture are usually employed [2], [3]. *Inner control loops* is employed for IBR-level control such as current-controller for grid-following (GFL)-based IBRs, voltage controller for grid-forming (GFM)-based IBRs, etc. *Primary control* is employed for stabilizing the voltage and frequency aftermath of an islanding event, for offering plug-n-play capability, and for maintaining proper share of the active and reactive power among multiple DERs, etc. *Secondary control* is employed to compensate the deviations in the voltage and frequency via dispatch rules, to control synchronization for seamlessly connection/disconnection of the MG to/from the grid, etc. *Tertiary control* is employed in energy-production and economic level that optimize and control the power flow between the MG and the grid.

In islanded mode of operation of MG, multiple IBRs are connected in parallel and each operates in GFM (part of the *inner control loops* control) and the droop-control method (part of the *primary control* control) is often applied in order to avoid circulating currents among the converters without using any critical communication between them. Reference [4] introduced the concept of *conventional droop controller* ($P\sim f$ and $Q\sim V$ droop law) for multiple inverters in dominantly inductive microgrid network by emulating the behavior of synchronous generators in traditional power systems. For other network conditions that arise in power distribution systems, several modifications on droop control are proposed that emphasize improved power sharing capabilities [5]–[9]. Although the *droop-based primary control* technique achieves high reliability and flexibility in successful stabilization of the MG, it causes the steady-state voltages and the frequency of the MG deviate from nominal values [5]–[7]. Moreover, due to asymmetrical connection of multiple GFM IBRs in the MG, the reactive power sharing between IBRs are not properly controlled via the *primary control* techniques alone [8], [9]. This naturally leads to importance of the *secondary control* that is usually attached with the *primary control* for resolving the aforementioned challenges. Articles [10]–[12] provide a comprehensive overview of the *secondary control* approaches (centralized, and distributed). In the centralized control technique, a centralized controller is utilized to compute the required adjustments/dispatch command for the *primary control* layers of each DERs [3]. The centralized communication link in between the central controller and the individual DER is required in this architecture [13]–[15]. The centralized approach makes the *secondary control* dispatching quite easy and results better and accurate control in frequency regulation, voltage regulation, reactive power sharing among the DERs due to proper coordination and accessibility of the global

This work was authored by the National Renewable Energy Laboratory, operated by Alliance for Sustainable Energy, LLC, for the U.S. Department of Energy (DOE) under Contract No. DE-AC36-08GO28308. Funding provided by the U.S Department of Energy Office of Energy Efficiency and Renewable Energy Solar Energy Technologies Office Agreement Number 38637. The views expressed in the article do not necessarily represent the views of the DOE or the U.S. Government. The U.S. Government retains and the publisher, by accepting the article for publication, acknowledges that the U.S. Government retains a nonexclusive, paid-up, irrevocable, worldwide license to publish or reproduce the published form of this work, or allow others to do so, for U.S. Government purposes.

information. However, this architecture is highly dependent on single central controller and enormous communication links that makes it more inclined to single-point failure of the communication results in complete failure of MG control [15]–[18]. To lessen the utilization of communication system the distributed *secondary control* has been proposed in many works that includes model predictive control (MPC) [19], adaptive control [20], deep reinforcement [21] and brain-emotional [22] learning based control, Koopman-inspired control [23], event-based control [24], finite-time control [25], cooperative control [26], multi-agent system (MAS)-employed consensus-based distributed algorithm [27]. Amongst the distributed approaches, the consensus algorithm is recognized as an appropriate method for the distributed control structure where every single controller communicates with other units via a mutual communication bus. Less communication stress and flexibility in nature makes this distributed *secondary control* more resistant to the communication failure at single-point [28], [29]. However, the complex mathematical computation in the consensus algorithm side along with the physical MG system dynamics makes the *secondary control* very complicated for the application in the real MG systems. Moreover, the inevitable latency and delay in the communication link deteriorate the overall system system stability [30]–[33]. Moreover, depending on the dispatch rule, multiple consensus algorithms are required to be run in parallel in order to ensure control in frequency regulation, voltage regulation, reactive power sharing among the DERs and that makes the *secondary control* complicated for practical usage [34]–[36].

Practical, vendor-neutral interoperability guidelines for the secondary control architecture of MGs incorporating multiple GFM-IBRs have not yet been established. This article proposes a generic, vendor-agnostic secondary control architecture compatible with all GFM IBRs and synchronous generators. The main contributions of this article are summarized as follows:

- This article addresses practical challenges associated with Modbus registers, including packet loss and quantization error, and their adverse effects on secondary control actions.
- The proposed modification strategies for any secondary control architecture, that includes data averaging, situational event-triggering of the controller, and finite iteration of the controlling action, mitigates these practical issues.
- The proposed secondary control architecture does not necessitate additional measurement devices within the MG and leverages the existing communication systems of GFM units, such as Modbus TCP/IP.

II. Secondary Control Architecture

A. Importance of Secondary Control

In this section, secondary control is discussed from the scope of reactive power sharing control among multiple GFM units in an islanded MG. Fig. 1 shows a generic MG consists of n number of GFM units connected to a common bus, point-of-common-coupling (PCC), via various lines. A complete description of the control typologies of the GFM units are out of scope; a brief description is provided. Each IBR-based GFM unit is controlled via voltage controller-based *inner control loop* where the reference voltage signal is generated using the P-f/Q-V droop control-based *primary control*. In case of a synchronous generator-based GFM unit, a P-f droop control-based *primary control* for the load-frequency controller (LFC) and a Q-V droop control-based *primary control* for the automatic voltage regulator (AVR) are used. For inductive lines, the *primary controller* without the *secondary control* specify the i^{th} GFM unit's frequency, ω_{i}, and voltage magnitude, V_{i} by:

$$\omega_{\text{i}} = \omega_{\text{nom}} - n_{\text{i}} P_{\text{i}}, \;\; V_{\text{i}} = V_{\text{nom}} - m_{\text{i}} Q_{\text{i}}, \tag{1}$$

where, ω_{nom}, V_{nom} are the nominal frequency (in rad/s) and voltage set-point (in volt) of the MG respectively. P_{i} and Q_{i} are the measured average active and reactive power of the i^{th} GFM unit, respectively. It is generated by processing the instantaneous active power, p_{i}, and reactive power, q_{i}, via a low-pass filters with the time constant, $\tau_{\text{S,i}} \in \mathbb{R}_{>0}$. As a result, $P_{\text{i}} := [1/(\tau_{\text{S,i}} s + 1)] p_{\text{i}}$ and $Q_{\text{i}} := [1/(\tau_{\text{S,i}} s + 1)] q_{\text{i}}$. The gains n_{i}, m_{i} are the droop coefficients. The large-signal stability analysis of the MG system yields the steady-state network

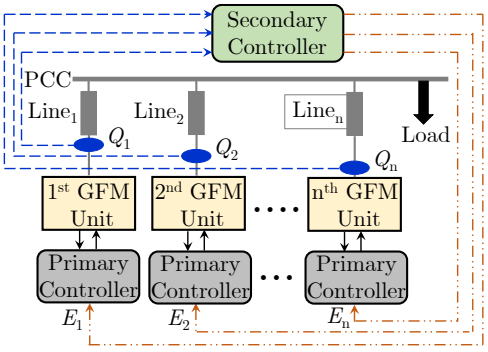

Fig. 1. Figure of centralized *secondary control* architecture on the top of the *primary control* layers for multiple GFM units connected in parallel.

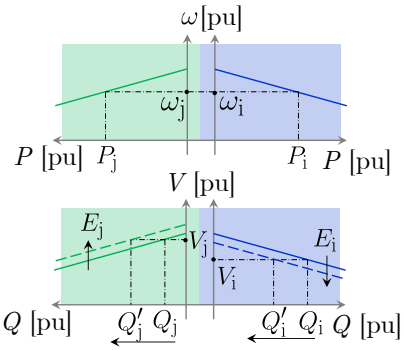

Fig. 2. Figure of P-f and Q-V droop-based *primary control* with *secondary control* for two parallel GFM units with equal ratings, connected to PCC through reactive lines with $X_{\text{j}} > X_{\text{i}}$.

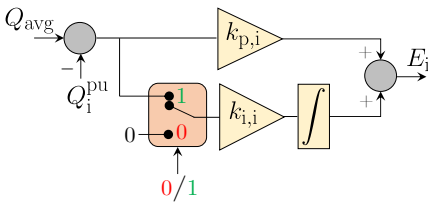

Fig. 3. Block diagram of proportional and integral regulator-based *secondary control* logic for reactive power sharing control.

frequency:

$$\omega_{\text{ss}} = \omega_{\text{nom}} - \frac{P_{\text{L}}}{\sum_{i=1}^{n}(1/n_{\text{i}})} \tag{2}$$

where P_{L} is the total active power load in the MG. The steady-state frequency, ω_{ss}, being a global quantity of the MG system, is different from the nominal ω_{nom}, but equal in all the GFM units. As a result, using the P-f droop law of eq. (1) and eq. (2), the following can be stated:

$$n_1 P_1 = n_2 P_2 = \ldots = n_{\text{i}} P_{\text{i}} = \ldots = n_{\text{n}} P_{\text{n}}. \tag{3}$$

Therefore, the total active power demand, P_{L}, is shared according to the selection of the P-f droop coefficients. In other words, the per-unitized active power with respect to each GFM unit's own base rating, are equal. This phenomenon is also possible to understand using the top figure of Fig. 2. However, the same analysis is not as straightforward as the previous case using large-signal stability analysis of the Q-V droop controller. It is well studied that due to the unequal line impedance effect, the Q-V droop controller is unable to share reactive power demand among even identical GFM units operating in parallel and as a result:

$$m_1 Q_1 \neq m_2 Q_2 \neq \ldots \neq m_{\text{i}} Q_{\text{i}} \neq \ldots \neq m_{\text{n}} Q_{\text{n}}. \tag{4}$$

For simplicity of exposition, a case study of two GFM units with identical ratings (i^{th} and j^{th} GFM unit), but operating through reactive lines with $X_{\text{j}} > X_{\text{i}}$ in parallel is considered. The bottom figure of Fig. 2 depicts the Q-V droop law before the *secondary control* action (solid lines of bottom figure of Fig. 2). The GFM units operate at voltages V_{i} and V_{j} with reactive power injections Q_{i} and Q_{j}. Since, $X_{\text{j}} > X_{\text{i}}$, the terminal voltages of the GFM units follows $V_{\text{i}} < V_{\text{j}}$ and as a result, reactive power flow follows $Q_{\text{i}} > Q_{\text{j}}$. This is the limitation of the employing only *primary control* without the *secondary control* compensation in case of parallel operation of multiple GFM units. Therefore, in order to ensure reactive power sharing amongst multiple GFM units connected to the PCC via asymmetrical lime impedances, a dynamic compensation of Q-V droop law is required. It is discussed in the next section elaborately.

B. Dynamic Compensation by the Secondary Control

The bottom figure of Fig. 2 shows that if the uncompensated Q-V droop curves (solid lines) are compensated in such a way that the droop curve for i^{th} and j^{th} GFM unit are moved down and up by E_{i} and E_{j}, respectively, the resulting steady-state reactive power output of both the GFM units become equal to each other, i.e., $Q_{\text{i}} = Q_{\text{j}}$. Therefore, the purpose of the *secondary control* layer is to determine the required compensation (E_{i} and E_{j} in this case) based on the measurement of the reactive power of the GFM units in the MG. As a result, for inductive lines the *primary controller* with the *secondary control* specify the i^{th} GFM unit's frequency, ω_{i}, and voltage magnitude, V_{i} by:

$$\omega_{\text{i}} = \omega_{\text{nom}} - n_{\text{i}} P_{\text{i}},\ V_{\text{i}} = V_{\text{nom}} - m_{\text{i}} Q_{\text{i}} + E_{\text{i}}. \tag{5}$$

Here without loosing the generality, a centralized *secondary control* layer is employed as shown in Fig. 1 where the *secondary control* layer receives reactive power outputs of all the GFM units (Q_1, Q_2, …, Q_{n}) and generates the compensating signals (E_1, E_2, …, E_{n}) and transmits to each GFM units. The *secondary control* action follows the following analytical steps:

`Step 1` : receive Q_1, Q_2, …, Q_{n} measurements from all GFM units and calculate per-unitized reactive power w.r.t. the own bases of GFM units such that:

$$Q_1^{\text{pu}} = \frac{Q_1}{S_1},\ Q_2^{\text{pu}} = \frac{Q_2}{S_2}, \ldots, Q_{\text{n}}^{\text{pu}} = \frac{Q_{\text{n}}}{S_{\text{n}}} \tag{6}$$

Here, S_1, S_2, …, S_{n} are the ratings of the GFM units.

`Step 2` : calculate $Q_{\text{avg}} := \frac{1}{n}(Q_1^{\text{pu}} + Q_2^{\text{pu}} + \ldots + Q_{\text{n}}^{\text{pu}})$.

`Step 3` : For compensation of i^{th} GFM units, compute:

$$E_{\text{i}} = k_{\text{p,i}}(Q_{\text{avg}} - Q_{\text{i}}^{\text{pu}}) + k_{\text{i,i}} \int (Q_{\text{avg}} - Q_{\text{i}}^{\text{pu}}) \text{d}t. \tag{7}$$

This is also shown in Fig. 3. Do this regulation operation form all the GFM units. In other words, *secondary control* layer consists of n number of such proportional and integral compensators to generate E_1, E_2, …, E_{n}.

`Step 4` : send E_1, E_2, …, E_{n} to GFM units for driving eq. (5).

The purpose of the $0/1$ bit of activation of the integral action will be discussed in Section IV. The compensating action in steady-state generates E_1, E_2, …, E_{n} in such a way that $Q_1^{\text{pu}} = Q_2^{\text{pu}} = \ldots = Q_{\text{i}}^{\text{pu}} = \ldots = Q_{\text{n}}^{\text{pu}} = Q_{\text{avg}}$. As a result, the per-unitized reactive power output of all the GFM units will be eventually equal to each other. This is equivalently true to state that after the compensations, eq. (4) becomes:

$$m_1 Q_1 = m_2 Q_2 = \ldots = m_{\text{i}} Q_{\text{i}} = \ldots = m_{\text{n}} Q_{\text{n}}. \tag{8}$$

III. Practical Challenges of Secondary Control

A. Motivation of the Proposed Secondary Control Architecture

It is clear from the previous section that the centralized *secondary control* architecture requires measurements of reactive power, Q_{i}'s, from each GFM unit in the MG and eventually the *secondary control* logic transmits compensating control signals, E_{i}'s, to each GFM units in the MG. The key targets of this work are to proposed a *secondary control* architecture among multiple GFM units:

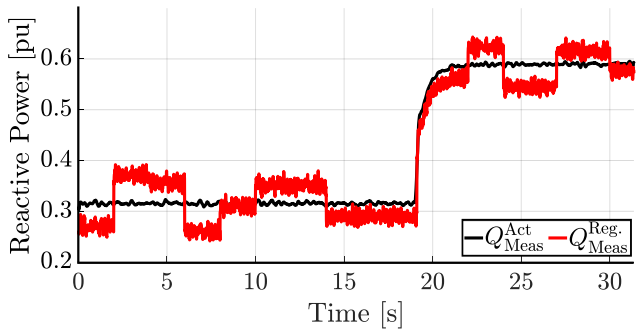

Fig. 4. Figure showing a sample where the reactive power measurement from the Modbus 'Holding Register' of a GFM unit under study, $Q^{\text{Reg.}}_{\text{Meas}}$, and from the DAQ using a accurate and precise external measurement device across the GFM unit, $Q^{\text{Act}}_{\text{Meas}}$.

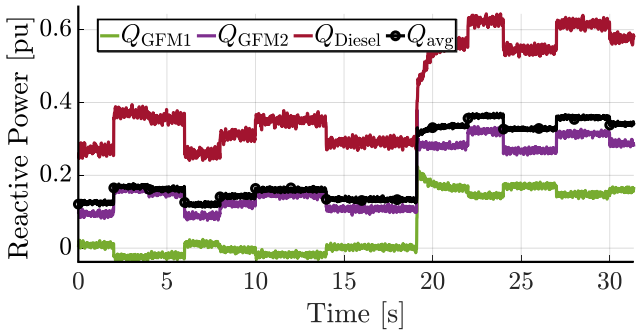

Fig. 5. Figure of reactive power measurement and the computed Q_{avg} based on `Step 2` with the sample from the Modbus 'Holding Register' of GFM units under study.

- without employing any additional measurement devices across multiple GFM units in the MG,
- utilization of the inherent communication system with which these commercial GFM units are equipped with.

These two requirements are very crucial in order achieve:

- the development of a GFM-unit-vendor-agnostic interoperability guidelines that would be useful for the end users and distribution system providers,
- the significant reduction of capital investments by the distribution system providers.

Most of the commercial GFM inverters from various vendors usually are equipped with standard communication protocols such as Modbus TCP/IP, RS-485 etc. Amongst many communication protocol, Modbus is the most widely available industrial protocol standard for controlling these commercial GFM inverters externally over Ethernet-based systems. It encapsulates the traditional Modbus data in a TCP/IP packet and stores the information in Modbus 'Holding Registers' so that the data can be read/write externally [37]. The advantage of the Modbus TCP/IP messaging protocol is its inherent simplicity and robustness (by retaining the message structure, register-based communication, etc.), reliability and interoperability.

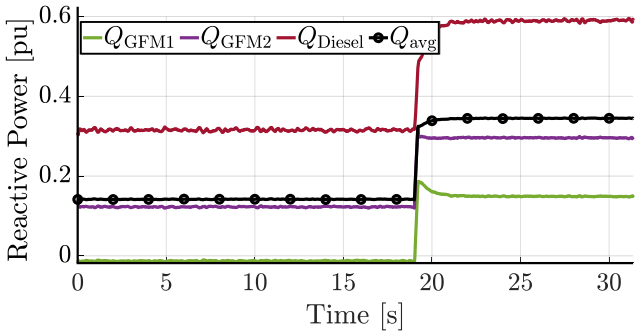

Fig. 6. Figure of reactive power measurement and the computed Q_{avg} based on `Step 2` with the sample from the DAQ across the GFM units.

B. Practical Challenges

Modbus TCP/IP messaging uses a low-bandwidth communication medium with high accuracy and precision of the transmitted data. In the application of the above-mentioned centralized *secondary control* architecture, where a continuous sampling to read data/measurements (i.e. Q_{i}) from the Modbus 'Holding Registers' and to send data/control signals (i.e. E_{i}) to the Modbus 'Holding Registers' of multiple GFM units, the data precision and accuracy can be significantly compromised due to various practical challenges that includes, packet lost, quantization error etc. [38]. For instance, Fig. 4 shows a sample where the reactive power measurement from the Modbus 'Holding Register' of a GFM unit under study, $Q^{\text{Reg.}}_{\text{Meas}}$, and from the data acquisition system (DAQ) using a accurate and precise external measurement device across the GFM unit, $Q^{\text{Act}}_{\text{Meas}}$ are shown. It is observed that due to continuous sampling (in this at each 10 ms), unlike the measurement from the DAQ, the data read from the Modbus register is having undesired but quite significant fluctuation due to the packet lost, quantization error and inevitable measurement high frequency noise. Although, the high-frequency measurement noise can be eliminated using the averaging phenomena on the sampled measurement, the less-frequent and significant-in-amount fluctuation due to the Modbus registers mal-operation, cannot be eliminated by the same.

C. Impact on the Secondary Control Logic

This less-frequent and significant-in-amount fluctuation due to the Modbus registers mal-operation deteriorates the dynamic compensation algorithm for *secondary control*. Due to the fluctuation in Q^{pu}_1, Q^{pu}_2, ..., Q^{pu}_{n} of `Step 1` (eq. (6)), as one sample is shown in Fig. 4, the step for computing the Q_{avg} (i.e. `Step 2`) experiences significant amount of fluctuation in the value. For instance, Fig. 5 shows the calculated Q_{avg} for the MG system under study consists of 3 GFM units using the data read from the Modbus registers of all the GFM units. Whereas, Fig. 6 shows the calculated Q_{avg} for the MG system under study using the data of DAQ. It is important to mention that change in Q_{avg} signifies the change in the total reactive power demand in the system. For example in Fig. 6, $Q_{\text{avg}} \approx 0$ till $t \approx 19$ s, as the total reactive

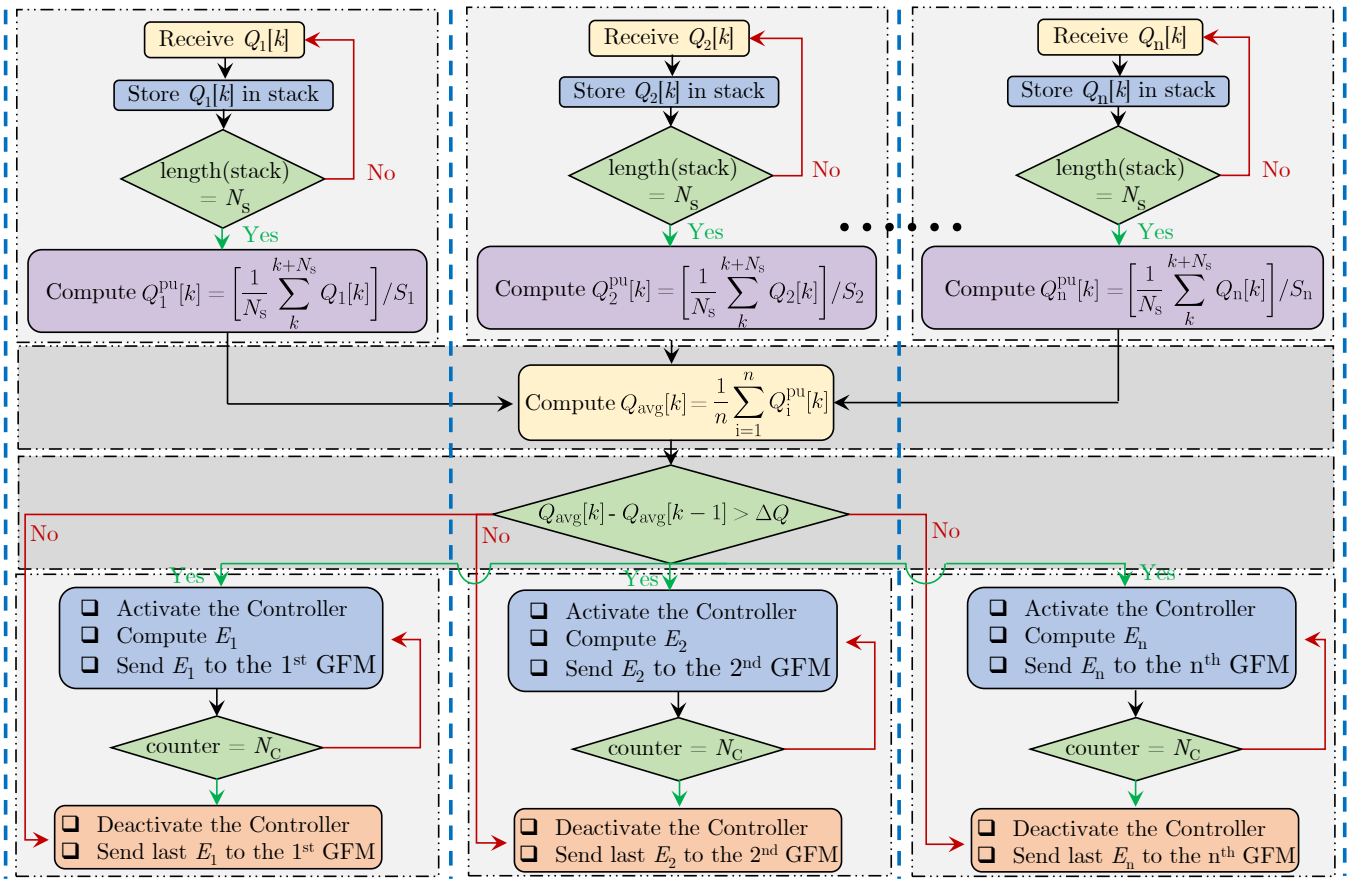

Fig. 7. Proposed modification for the *secondary control* with averaging the data read, event-triggering and finite iteration.

power demand is 0. The small non-zero value of Q_{avg} is due to inherent line inductive reactive power loss by the small circulating current between GFM units. It changes at $t \approx 19$ s when there is a jump in reactive power demand in the system. However, in case of Fig. 5, the Q_{avg} jumps up and down from the actual value quite significantly in this similar situation. As Q_{avg} works as reference signal for the proportional and integral regulator (eq. (7) and Fig. 3), it will eventually generate a fluctuating compensating signals (i.e. E_1, E_2, ..., E_n of `Step 3`) and never reach steady-state even though the reactive power demand doesn't fluctuates. This is indeed a quite practical challenge that needs to be resolved for the real-world application.

IV. Proposed Modifications for the Algorithm

A three-stage modification in the *secondary control* architecture and the algorithm is proposed, as shown in Fig. 7, in order to resolve these practical challenges. These stages are as follows:

A. Averaging the Measurements after Data Read

This is a minor stage where the primary target is to eliminate the high-frequency measurement noises generated in the measurements of reactive power from the Modbus registers. It is done by defining a 'stack' of order N_S as shown in Fig. 7. Let say, $Q_i[k]$ is the sampled data read from the 'Holding Register' of the i^{th} GFM unit at a sample rate of T_S ms. As a result, the following computation is done and transmitted to the further into the algorithm at each $N_S T_S$ ms:

$$Q_i^{pu}[k] = \left[\frac{1}{N_S}\sum_{k}^{k+N_S} Q_i[k]\right]/S_i. \tag{9}$$

The sampling time for the data read from the register, T_S, and the stack length, N_S, can be selected from outside based on the application by the end user. In this study, T_S and N_S are selected to be 10 ms and 100, respectively. As a result, the computed Q_i^{pu} is further send to the algorithm as 1 s interval.

B. Situational Event-triggering of the Algorithm

This is one of the major stages where the primary target (along with the next stage) is to eliminate the impact of fluctuation of the Q_i^{pu} due to the Modbus registers maloperation. It is done by defining a 'conditional check' such as $Q_{avg}[k] - Q_{avg}[k-1] > \Delta Q$, as shown in Fig. 7. $Q_{avg}[k]$ is computed using the logic of `Setp 2`, also shown in Fig. 7. Note that $Q_{avg}[k]$ and $Q_{avg}[k-1]$ are separated by $N_S T_S$ second due to the previous averaging. If this condition check is satisfied, then it triggers an activation signal (a single bit 0/1) to the integral action of the proportional and integral controller of Fig. 3. Note that Q_{avg} is an indicator of the total

reactive power demand of the MG as sum of the generated reactive power by the GFM units is equal (slightly more due to reactive power losses of the MG network) the total reactive power demand. However, due to the mal-operation of Modbus registers, Q_{avg} continuously changes even after $N_{\text{S}}T_{\text{S}}$ second, as shown empirically in Fig. 5. Therefore, the value of the ΔQ should be selected judiciously, configurable for the end users, in order to distinguish the change in Q_{avg} caused by either the true change in the reactive power demand in MG or the fluctuating value computed from the data read from the mal-operated Modbus registers. In other words, ΔQ should be high enough to distinguish the reactive power demand change and the fluctuation due to the erroneous Modbus values. On the other hand, it should be low enough to trigger the controller when a reasonable amount of reactive power is changed truly in the MG. In this study, ΔQ is selected to be 1% in p.u.

C. Finite Iteration of the Compensation of the Algorithm

This is the last major stage where the primary target (along with the previous stage) is to eliminate the impact of fluctuation of the Q_{i}^{pu} due to the Modbus registers mal-operation. Once the integral action is activated by the event-triggering signal of the previous stage, it starts computing E_{i} and is transmitted to the i^{th} GFM unit's corresponding Modbus 'Holding Register'. However, a conditional check runs in parallel to count the number of iteration of the controller, 'counter' of the Fig. 7. Once the condition counter $= N_{\text{C}}$ is satisfied, the controller gets deactivated by sending 0 bit, as shown in Fig. 3. In other words, the controller action runs for finite N_{C} iteration before getting deactivated. This stage ensures not to send control signals to the Modbus 'Holding Registers' continuously one sufficient close reactive power sharing is achieved. As a result, the 'Holding Registers' will be latched to the last control signals, E_{i}, sent by the algorithm. The value of the N_{C} should be selected judiciously and it mostly depends on the aggressiveness of the controller action (determined by the value of $k_{\text{p,i}}$ and $k_{\text{i,i}}$ of Fig. 3) selected by the end users. In this study, with a selection of $k_{\text{p,i}} = 0.01$ and $k_{\text{i,i}} = 1.5$, N_{C} is selected to be 2.

V. Hardware-based Experimental Validation

A. Hardware Setup Under Study

Fig. 8(a) and Fig. 8(b) show the overall laboratory-based experimental setup of MG system. It consists of two 3-ϕ, 480 V, 60 Hz commercial GFM IBRs (GFM-1 of 250 kVA and GFM-2 of 125 kVA rating), one 3-ϕ, 480 V, 60 Hz commercial diesel generator (Gen-set of 187.5 kVA rating), and a load bank of 500 kVA. GFM-1 and GFM-2 are connected to the common bus, PCC, via 3-ϕ, $480/480$ V, 60, Δ-Y transformers of rating of 500 kVA and 250 kVA, and and transformer reactance of 4.5% p.u. and 5% p.u., respectively. For all the GFM units, the P-f droop coefficient is 0.6% and Q-V droop coefficient is 5%. All GFM units are compatible with Modbus TCP/IP communication that allows Modbus devices to communicate over Ethernet. The proposed modified *secondary control* logic is developed using Python 3.7.1, and

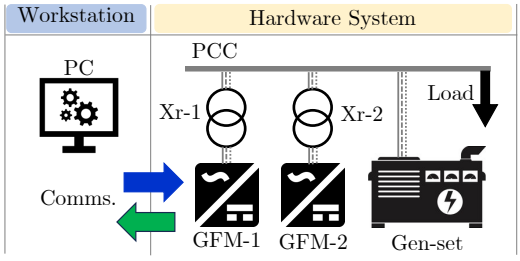

(a)

(b)

Fig. 8. Laboratory-based experimental setup of microgrid system.

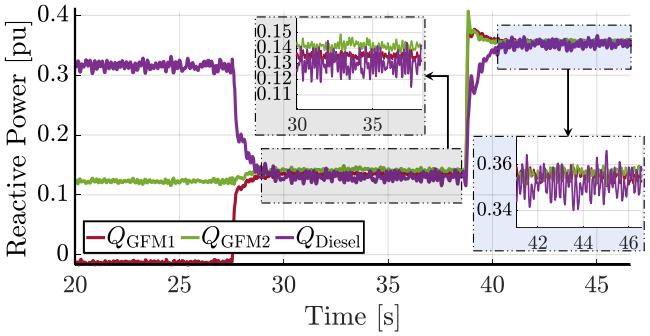

Fig. 9. Results of reactive power sharing among GFM-1, GFM-2, and Gen-set of Fig. 8(a) with the proposed modifications in the centralized secondary control algorithm.

is running on a server workstation. Therefore, the workstation receives all the measured reactive power from each GFM units via accessing the in-built dedicated Modbus registers and sends the compensating signals to the GFM units directly to the in-built dedicated Modbus register. No additional sensors/measurements are required for this operation of the proposed modified *secondary control* logic. However, the test system is equipped with additional sensors for precise and accurate DAQ and visualization.

B. Experimental Results and Discussions

In this test case, the total active, P_{Load}, and reactive, Q_{Load}, power are 300 kW throughout and 100 kVAr until $t \approx 38$ s and 200 kVAr after $t \approx 38$ s, respectively. Fig. 9 shows that the reactive power sharing among the GFM units is unequal until

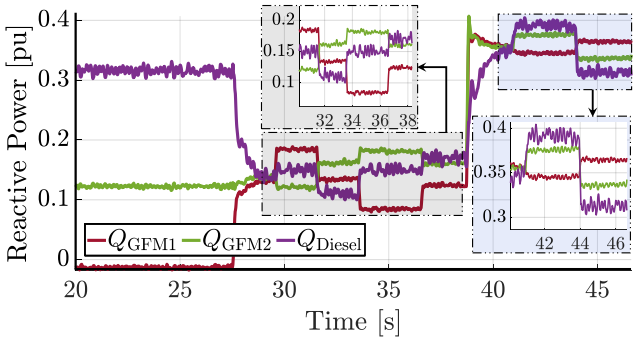

Fig. 10. Results of reactive power sharing among GFM-1, GFM-2, and Gen-set of Fig. 8(a) without the proposed modifications in the centralized secondary control algorithm.

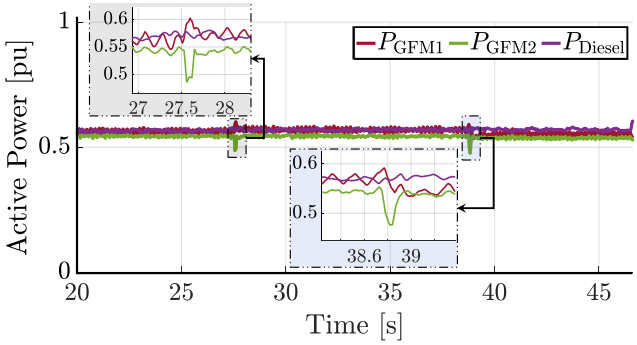

Fig. 12. Results of active power sharing among GFM-1, GFM-2, and Gen-set of Fig. 8(a) with the proposed modifications in the centralized secondary control algorithm.

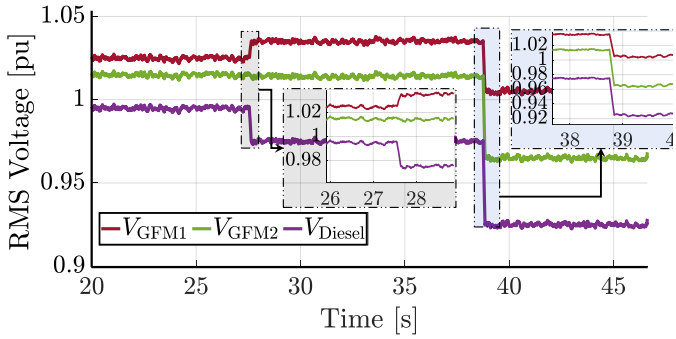

Fig. 11. Results of RMS of terminal voltages of GFM-1, GFM-2, and Gen-set of Fig. 8(a) with the proposed modifications in the centralized secondary control algorithm.

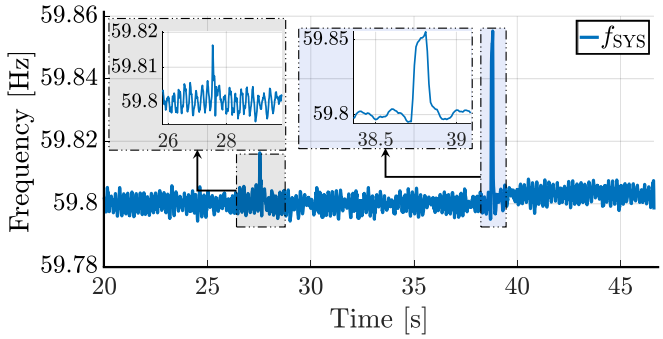

Fig. 13. Results of frequency of the MG of Fig. 8(a) with the proposed modifications in the centralized secondary control algorithm.

$t \approx 26$ s because the secondary control is not applied; however, at $t \approx 26$ s, the p.u. reactive power of all GFM units becomes equal as the secondary control with the proposed modification is employed. The equal reactive power sharing capability continues after $t \approx 38$ s, when the load demand increases in the MG. Fig. 10 shows that the reactive power sharing among the GFM units is unequal until $t \approx 26$ s because the secondary control is not applied; however, at $t \approx 26$ s, the p.u. reactive power of all GFM units come closer to each other but fluctuates and never reach a steady-state as the secondary control is employed without the proposed modifications. It is observed that without the proposed modification, even after $t \approx 26$ s, the secondary control initially attempts equal reactive power sharing, but due to the Modbus register errors, the Q_{avg} is continuously fluctuating, and therefore we observe fluctuating reactive power sharing throughout the experiment. The equal reactive power sharing capability with significant fluctuation continues after $t \approx 38$ s, when the load demand increases in the MG. This shows the advantage of the proposed modification of the secondary control logic for practical usage under such erroneous measurements.

Fig. 11 shows the resulting root-mean-square (RMS) voltage at the terminals of the GFM units, caused by the compensations of the secondary control. It is observed that the secondary control algorithm with the proposed modifications determines the corrective amount of adjustments for the V-Q droop curves of the GFM units (i.e., E_1, E_2, and E_3 for GFM-1, GFM-2, and Gen-set, respectively). These adjustments changes the terminal RMS voltage of each GFM units in the MG system to make the reactive sharing equal with respective to each GFM units rating. The equal reactive power sharing capability with significant fluctuation continues after $t \approx 38$ s, when the load demand increases in the MG by generating new sets of E_1, E_2, and E_3 for GFM-1, GFM-2, and Gen-set, respectively.

Fig. 13 and Fig. 12 show the frequency of the entire MG system and the active power during sharing among the GFM units under this scenario of employing the proposed modifications in the centralized secondary control algorithm, respectively. These results show that the proposed secondary control does not effect the active power sharing and the frequency of the MG system.

VI. Conclusion

A *secondary control* framework for microgrids, utilizing existing communication systems like Modbus TCP/IP, is proposed that doesn't require extra measurement devices. Challenges such as packet loss and Modbus holding register errors significantly impact *secondary control* effectiveness. To address this, a three-stage modification approach is suggested, involving data averaging, event-triggered control, and iterative action. The effectiveness of this method is demonstrated

using a real-world laboratory microgrid setup with commercial communication units. This cost-effective approach offers guidelines for *secondary control* in microgrids, beneficial for distribution system providers.

REFERENCES

[1] "IEEE standard for the specification of microgrid controllers," *IEEE Std 2030.7-2017*, pp. 1–43, 2018.

[2] J. M. Guerrero, J. C. Vasquez, J. Matas, L. G. De Vicuña, and M. Castilla, "Hierarchical control of droop-controlled ac and dc microgrids—a general approach toward standardization," *IEEE Transactions on industrial electronics*, vol. 58, no. 1, pp. 158–172, 2010.

[3] A. Bidram and A. Davoudi, "Hierarchical structure of microgrids control system," *IEEE Transactions on Smart Grid*, vol. 3, no. 4, pp. 1963–1976, 2012.

[4] M. C. Chandorkar, D. M. Divan, and R. Adapa, "Control of parallel connected inverters in standalone ac supply systems," *IEEE Transactions on Industry Applications*, vol. 29, no. 1, pp. 136–143, 1993.

[5] J. M. Guerrero, L. G. De Vicuna, J. Matas, M. Castilla, and J. Miret, "A wireless controller to enhance dynamic performance of parallel inverters in distributed generation systems," *IEEE Transactions on power electronics*, vol. 19, no. 5, pp. 1205–1213, 2004.

[6] Q.-C. Zhong, "Robust droop controller for accurate proportional load sharing among inverters operated in parallel," *IEEE Transactions on Industrial Electronics*, vol. 60, no. 4, pp. 1281–1290, 2011.

[7] D. K. Dheer, Y. Gupta, and S. Doolla, "A self-adjusting droop control strategy to improve reactive power sharing in islanded microgrid," *IEEE Transactions on Sustainable Energy*, vol. 11, no. 3, pp. 1624–1635, 2020.

[8] Y. Ling, Y. Li, Z. Yang, and J. Xiang, "A dispatchable droop control method for distributed generators in islanded ac microgrids," *IEEE Transactions on Industrial Electronics*, pp. 1–1, 2020.

[9] S. Chakraborty, S. Patel, G. Saraswat, A. Maqsood, and M. V. Salapaka, "Seamless transition of critical infrastructures using droop-controlled grid-forming inverters," *IEEE Transactions on Industrial Electronics*, vol. 71, no. 2, pp. 1535–1546, 2024.

[10] F. Nawaz, E. Pashajavid, Y. Fan, and M. Batool, "A comprehensive review of the state-of-the-art of secondary control strategies for microgrids," *IEEE Access*, 2023.

[11] Y. Khayat, Q. Shafiee, R. Heydari, M. Naderi, T. Dragičević, J. W. Simpson-Porco, F. Dörfler, M. Fathi, F. Blaabjerg, J. M. Guerrero *et al.*, "On the secondary control architectures of ac microgrids: An overview," *IEEE Transactions on Power Electronics*, vol. 35, no. 6, pp. 6482–6500, 2019.

[12] O. F. Rodriguez-Martinez, F. Andrade, C. A. Vega-Penagos, and A. C. Luna, "A review of distributed secondary control architectures in islanded-inverter-based microgrids," *Energies*, vol. 16, no. 2, p. 878, 2023.

[13] G. Yao, Y. Lu, T. Tang, M. Benbouzid, Y. Zheng, and T. Wang, "A central control strategy of parallel inverters in ac microgrid," in *IECON 2013-39th Annual Conference of the IEEE Industrial Electronics Society*. IEEE, 2013, pp. 7112–7117.

[14] A. Micallef, M. Apap, C. Spiteri-Staines, J. M. Guerrero, and J. C. Vasquez, "Reactive power sharing and voltage harmonic distortion compensation of droop controlled single phase islanded microgrids," *IEEE Transactions on Smart Grid*, vol. 5, no. 3, pp. 1149–1158, 2014.

[15] M. Savaghebi, A. Jalilian, J. C. Vasquez, and J. M. Guerrero, "Secondary control for voltage quality enhancement in microgrids," *IEEE Transactions on Smart Grid*, vol. 3, no. 4, pp. 1893–1902, 2012.

[16] K. T. Tan, X. Peng, P. L. So, Y. C. Chu, and M. Z. Chen, "Centralized control for parallel operation of distributed generation inverters in microgrids," *IEEE Transactions on Smart Grid*, vol. 3, pp. 1977–1987, 2012.

[17] J. P. Lopes, C. L. Moreira, and A. Madureira, "Defining control strategies for microgrids islanded operation," *IEEE Transactions on power systems*, vol. 21, no. 2, pp. 916–924, 2006.

[18] Y. A.-R. I. Mohamed and A. A. Radwan, "Hierarchical control system for robust microgrid operation and seamless mode transfer in active distribution systems," *IEEE Transactions on Smart Grid*, vol. 2, no. 2, pp. 352–362, 2011.

[19] E. D. Escobar, D. Betancur, T. Manrique, and I. A. Isaac, "Model predictive real-time architecture for secondary voltage control of microgrids," *Applied Energy*, vol. 345, p. 121328, 2023.

[20] N. M. Dehkordi, N. Sadati, and M. Hamzeh, "Fully distributed cooperative secondary frequency and voltage control of islanded microgrids," *IEEE Transactions on Energy Conversion*, vol. 32, no. 2, pp. 675–685, 2016.

[21] P. I. d. N. Barbalho, V. Lacerda, R. Fernandes, and D. V. Coury, "Deep reinforcement learning-based secondary control for microgrids in islanded mode," *Electric Power Systems Research*, vol. 212, p. 108315, 2022.

[22] M. S. O. Yeganeh, A. Oshnoei, N. Mijatovic, T. Dragicevic, and F. Blaabjerg, "Intelligent secondary control of islanded ac microgrids: A brain emotional learning-based approach," *IEEE Transactions on Industrial Electronics*, vol. 70, no. 7, pp. 6711–6723, 2022.

[23] X. Gong and X. Wang, "A novel koopman-inspired method for the secondary control of microgrids with grid-forming and grid-following sources," *Applied Energy*, vol. 333, p. 120631, 2023.

[24] G. Lou, W. Gu, J. Wang, W. Sheng, and L. Sun, "Optimal design for distributed secondary voltage control in islanded microgrids: Communication topology and controller," *IEEE Transactions on Power Systems*, vol. 34, no. 2, pp. 968–981, 2018.

[25] Z. Deng, Y. Xu, H. Sun, and X. Shen, "Distributed, bounded and finite-time convergence secondary frequency control in an autonomous microgrid," *IEEE Transactions on Smart Grid*, vol. 10, no. 3, pp. 2776–2788, 2018.

[26] A. Bidram, A. Davoudi, F. L. Lewis, and J. M. Guerrero, "Distributed cooperative secondary control of microgrids using feedback linearization," *IEEE transactions on power systems*, vol. 28, no. 3, pp. 3462–3470, 2013.

[27] Q. Shafiee, J. M. Guerrero, and J. C. Vasquez, "Distributed secondary control for islanded microgrids—a novel approach," *IEEE Transactions on power electronics*, vol. 29, no. 2, pp. 1018–1031, 2013.

[28] E. Espina, R. Cárdenas-Dobson, J. W. Simpson-Porco, M. Kazerani, and D. Sáez, "A consensus-based distributed secondary control optimization strategy for hybrid microgrids," *IEEE Transactions on Smart Grid*, 2023.

[29] Y. Zhang, A. M. Shotorbani, L. Wang, and B. Mohammadi-Ivatloo, "Distributed secondary control of a microgrid with a generalized pi finite-time controller," *IEEE Open Access Journal of Power and Energy*, vol. 8, pp. 57–67, 2021.

[30] A. Lasheen, H. F. Sindi, M. Nour, M. Shaaban, A. Osman, and H. H. Zeineldin, "Impact of secondary control design on the microgrid domain of stability considering reactive power sharing," *IEEE Access*, 2023.

[31] C. Liu, X. Wang, T. Yao, and X. Wang, "Self-triggered $\mathcal{H}_\infty$ consensus-based secondary control of ac microgrids with uncertainty of communication," *International Journal of Electrical Power & Energy Systems*, vol. 145, p. 108679, 2023.

[32] E. A. Coelho, D. Wu, J. M. Guerrero, J. C. Vasquez, T. Dragicević, C. Stefanović, and P. Popovski, "Small-signal analysis of the microgrid secondary control considering a communication time delay," *IEEE Transactions on Industrial Electronics*, vol. 63, no. 10, pp. 6257–6269, 2016.

[33] G. Lou, W. Gu, Y. Xu, W. Jin, and X. Du, "Stability robustness for secondary voltage control in autonomous microgrids with consideration of communication delays," *IEEE Transactions on Power Systems*, vol. 33, no. 4, pp. 4164–4178, 2017.

[34] J. W. Simpson-Porco, Q. Shafiee, F. Dörfler, J. C. Vasquez, J. M. Guerrero, and F. Bullo, "Secondary frequency and voltage control of islanded microgrids via distributed averaging," *IEEE Transactions on Industrial Electronics*, vol. 62, no. 11, pp. 7025–7038, 2015.

[35] J. Liu, J. Li, H. Song, A. Nawaz, and Y. Qu, "Nonlinear secondary voltage control of islanded microgrid via distributed consistency," *IEEE Transactions on Energy Conversion*, vol. 35, no. 4, pp. 1964–1972, 2020.

[36] E. Espina, R. Cárdenas-Dobson, J. W. Simpson-Porco, M. Kazerani, and D. Sáez, "A consensus-based distributed secondary control optimization strategy for hybrid microgrids," *IEEE Transactions on Smart Grid*, 2023.

[37] N. Goldenberg and A. Wool, "Accurate modeling of modbus/tcp for intrusion detection in scada systems," *international journal of critical infrastructure protection*, vol. 6, no. 2, pp. 63–75, 2013.

[38] M. Faisal, A. A. Cardenas, and A. Wool, "Modeling modbus tcp for intrusion detection," in *2016 IEEE Conference on Communications and Network Security (CNS)*. IEEE, 2016, pp. 386–390.